An upscaling model for simulation of geothermal processes in stratified formations

Tang, Jinyu; Wang, Yang; Rossen, William R.

DOI
10.1016/j.geothermics.2024.103095

Publication date
2024

Document Version
Final published version

Published in
Geothermics

Geothermics 122 (2024) 103095

Contents lists available at ScienceDirect

Geothermics

journal homepage: www.elsevier.com/locate/geothermics

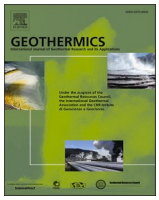

An upscaling model for simulation of geothermal processes in stratified formations

Jinyu Tang [a,*], Yang Wang [b,**], William R. Rossen [c]

[a] Department of Chemical and Petroleum Engineering, United Arab Emirates University, Al Ain, Abu Dhabi, 15551, United Arab Emirates
[b] Department of Civil Engineering, Qingdao University of Technology, Jialingjiang Road 777, Qingdao, 266520, China
[c] Department of Geoscience and Engineering, Delft University of Technology, Stevinweg 1, Delft, 2628CN, the Netherlands

ARTICLE INFO

Key words:
Heterogeneity
Thermal Taylor dispersion
Geothermal modeling
Upscaling
Thermophysical properties

ABSTRACT

In stratified porous media, non-uniform velocity between layers combined with thermal conduction across layers causes spreading of the thermal front: thermal Taylor dispersion. Conventional upscaling not accounting for this heterogeneity within simulation grid blocks underestimates thermal dispersion, leading to overestimation of thermal breakthrough time. We derive a model for effective longitudinal thermal diffusivity in the direction of flow, α_{eff}, to represent the effective thermal dispersion in two-layer media. α_{eff}, accounting for thermal Taylor dispersion, is much greater than the thermal diffusivity of the rock itself. We define a dimensionless number, N_{TC}, a ratio of times for longitudinal convection to transverse conduction, as an indicator of transverse thermal equilibration of the system during cold- or hot-water injection. For $N_{TC} > 5$, thermal dispersion in the two-layer system closely approximates a single layer with α_{eff}. This suggests a two-layer medium satisfying $N_{TC} > 5$ can be combined into a single layer with an effective longitudinal thermal diffusivity α_{eff}. In application to a geothermal reservoir, one can apply the model to perform upscaling in stages, i.e. combining two layers satisfying the N_{TC} criterion in each stage. The α_{eff} model accounting for the fine-scale heterogeneity within simulation grid blocks would enhance the prediction accuracy of thermal breakthrough time and thus thermal lifetime.

1. Introduction

Geothermal formations usually feature strong heterogeneity (Blank et al., 2021; Crooijmans et al., 2016; Major et al., 2023). In numerical simulations of geothermal processes, a full description of fine-scale heterogeneity using fine-grid resolution is computationally expensive. It is necessary to upscale the description of formation heterogeneity, utilizing large grid blocks and assigning uniform properties within each grid block. Conventional upscaling estimates geophysical properties within a grid block by averaging: e.g. arithmetic, harmonic or geometric averaging (Norouzi et al., 2022; Plumb and Whitaker, 1988; Thomas et al., 2023). These averaging methods yield upscaled thermal conductivities close to conductivities of rock itself (Rühaak et al., 2015). This way of upscaling is often problematic, because formation heterogeneity strongly affects thermal dispersion (Robert et al., 2022) but is not accounted for in the upscaled thermo-physical properties. This leads to inaccurate prediction of thermal breakthrough time. Our goal is to develop a more-effective approach for upscaling: specifically, of thermo-physical properties of rocks. In particular, we account for the effect of fine-scale heterogeneity of layers combined within simulation grid blocks in our new upscaling approach.

Taylor (1953) analyzed the concentration distribution of solute in a liquid flowing slowly through a tube. The spreading of the concentration distribution results from combined effects of convection and longitudinal and transverse diffusion (Dentz et al., 2018; Taylor, 1953). The transverse diffusion arises from velocity variations in the vertical cross-section, as shown in Fig. 1a., shrinking the concentration spreading that would result from convection alone. This phenomenon is known as Taylor dispersion. It has been extensively studied in various bulk and subsurface processes, e.g. transport of contaminant or radioactive waste, mixing of oil-displacing agents or dispersion of a tracer. The spreading of solute concentration in the flow direction is dominated by Taylor dispersion from non-uniform convection and transverse diffusion across streamlines. John et al. (2010) also illustrate that for field-scale mixing in heterogeneous formations, velocity variation between layers together with transverse diffusion across layers is primarily dominant over longitudinal diffusion. This indicates that ignoring

* Corresponding author.
** Co-corresponding author.
E-mail addresses: j.tang@uaeu.ac.ae (J. Tang), wangyang_1990@outlook.com (Y. Wang).

https://doi.org/10.1016/j.geothermics.2024.103095
Received 29 August 2023; Received in revised form 18 June 2024; Accepted 24 June 2024
Available online 4 July 2024

Nomenclature

e_c = heat flux in the flow direction by transverse conduction, J/(s.K)
(e_{tj}/e_{lj}) = ratio of heat fluxes driven by transverse conduction and longitudinal convection, dimensionless (Eqs. 10 and 11)
F_h = fraction of total thickness in the high-permeability layer
F_c = heat-capacity contrast between layers
F_{ch} = heat capacity-thickness contrast between layers
F_K = permeability contrast between layers
H = total reservoir thickness in z direction, m
h_j = layer thickness in z direction, m
I_{TC} = transverse thermal-conduction index, dimensionless (Eq. 27)
j = layer index
K_j = permeability, m^2
L = reservoir length, m
N_{TC} = transverse thermal conduction number, dimensionless (Eq. 13)
$(N_{pe})^{-1}$ = inverse Péclet number, dimensionless (Eq. 23)
$(N_{pe}^{eff})^{-1}$ = effective inverse Péclet number, dimensionless (Eq. 31)
Q_D = dimensionless injection time (Eq. 1)
$(Q_{D0})_{TD=0.5}$ = cumulative heat injection at the breakthrough of T_D = 0.5 without heat conduction in either direction, dimensionless (Eq. 1)
$(Q_D)_{TD=0.5}$ = cumulative heat injection at the breakthrough of T_D = 0.5 with heat conduction, dimensionless (Eq. 1)
T = temperature, °C
T_{inj}, T_{ini} = injection and initial temperature, °C
T_D = dimensionless temperature (Eq. 1)
t = cold-water injection time, s
t_{lj} = convection-driven thermal-front breakthrough time, s
t_{tj} = transverse thermal-conduction time across the two layers, s
u_j = Darcy velocity of cold-water injection, m/s
$\bar{v}$ = heat capacity-thickness weighted average convection velocity of the cooling-front in a two-layer system, m/s (Eq. 5)
v_j = convection velocity of the cooling front, m/s
W = reservoir width, m
x, y, z = Cartesian coordinates, m
x_D = dimensionless position in x direction (Eq. 1)
$\hat{x}_D$ = dimensionless position relative to a plane moving at $\bar{v}$ (Eq. 15)
z_D = dimensionless position in z direction (Eq. 1)
α_{lj}, α_{tj} = longitudinal and transverse thermal diffusivity, m^2/s
$\bar{\alpha}_l$ = thickness-weighted average of longitudinal diffusivities α_{l1} and α_{l2}, m^2/s
α_{eff} = effective longitudinal thermal diffusivity, m^2/s (Eqs. 24 and 25)
κ_{lj}, κ_{tj} = longitudinal and transverse thermal conductivity, W/(m.K)
κ_{eff} = effective longitudinal thermal conductivity, W/(m.K)
$(\overline{\rho c_p})$ = thickness-weighted average heat capacity, J/(m^3.K) (Eq. 3)
$(\rho c_p)_j$ = layer heat capacity accounting for rock grains and fluids, J/(m^3.K) (Eq. 2)
$(\rho_w c_{pw})$ = heat capacity of water, J/(m^3.K)
$(\rho_{gj} c_{pgj})$ = heat capacity of rock grains, J/(m^3.K)
ϕ_j = porosity, dimensionless

longitudinal diffusion may cause little or no loss of accuracy in the modeling of dispersion.

Thermal dispersion in stratified geothermal formations exhibits a similar phenomenon: velocity variations between layers result in non-uniform thermal fronts, illustrated in Fig. 1b. This causes transverse thermal conduction across layers, which reduces the spreading of the cooling front: thermal Taylor dispersion (Bruderer and Bernabé, 2001; Emami Meybodi and Hassanzadeh, 2011; Yan et al., 2022). In effect, thermal Taylor dispersion slows down the advance of the leading edge of the cooling front. This is especially crucial in that the advance of the cooling front dominates the thermal lifetime of a geothermal process and thus production of geothermal energy (Sbai and Larabi, 2023).

This phenomenon has been addressed in various thermal processes, e.g. wellbore heat transmission in the petroleum industry or transportation of geothermal fluids for heating (Batycky et al., 1994; Ortan et al., 2009; Park et al., 2018; Tang and van der Zee, 2021). In these processes, the major cause for thermal Taylor dispersion is velocity variation within a pipe or channel (e.g., Nakayama et al., 2006; Pearce and Daou, 2014). However, no model has yet accounted for Taylor dispersion of the temperature front in vertically heterogeneous porous media.

We investigate the effect of heterogeneity within a geothermal reservoir on thermal dispersion (Bredesen et al. 2020; Seibert et al., 2014; Wang et al., 2020). Heat conduction from the overburden and underburden rocks affects the advance of the cooling front inside a reservoir (Willems et al., 2017; De Bruijn et al., 2021), but is neglected here for simplification. The approach we deploy is similar to that of Lake and Hirasaki (1981) for chemical dispersion. Nevertheless, heat conduction is different from chemical diffusion, especially in that heat conduction is through both fluid and surrounding rocks and its dispersion coefficient is of order ~ 10^{-6} m^2/s, about 10^3 times greater than chemical-diffusion coefficient in liquids (~ 10^{-9} m^2/s). Our goals are (1) to define a measure of the effects of transverse thermal conduction and (2) develop a model to represent effective thermal dispersion in layered

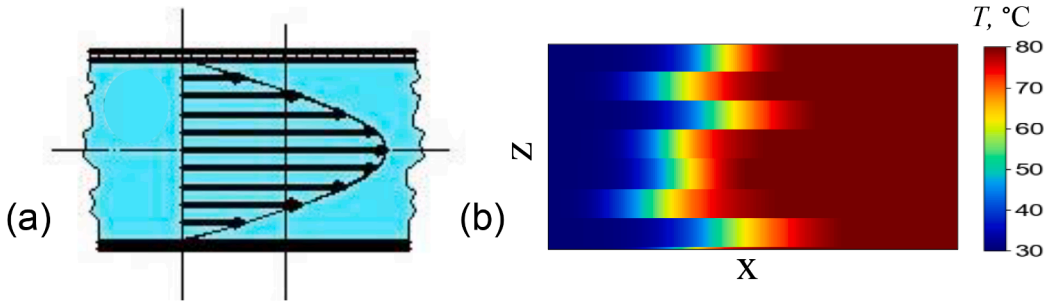

Fig. 1. (a) Fluid-velocity profile in cross-section during fluid flow through a pipe (adapted from Wikipedia, 2016) and **(b)** Non-even cooling fronts between layers upon cold-water injection into a hot-water-saturated multi-layer porous medium (van Nieuwkerk, 2022).

porous media. In particular, we define a dimensionless criterion for combining a two-layer medium. Then we derive an analytical model for effective thermal diffusivity to represent the effective dispersion in the combined system. At the end, we illustrate the application of the model to upscaling the well-log data of a geothermal reservoir. More application examples are presented in van Nieuwkerk (2022).

2. Geological model, assumptions and definitions

2.1. Two-layer geological model

Fig. 2a shows the well-log data from a geothermal reservoir featuring a pattern of layers. The thermal Taylor dispersion theory for upscaling is developed based on a two-layer system that represents such a sequence, as shown in Fig. 2b. We examine two representative scenarios: (1) two permeable layers with a permeability contrast and (2) two layers with one layer impermeable.

Each layer $j = 1$ or 2 is characterized by the following properties: h_j – thickness in the z direction, ϕ_j – porosity, K_j – permeability, and α_{lj} and α_{tj} – longitudinal and transverse thermal diffusivity. Respectively, α_{lj} and α_{tj} are ratios of thermal conductivity in the given direction to heat capacity, i.e., $[\kappa_{lj}/(\rho_{Cp})_j]$ and $[\kappa_{tj}/(\rho_{Cp})_j]$ with j =1 denoting the higher-permeability layer.

2.2. Assumptions and definitions

For the analysis of thermal Taylor dispersion, we have made the following simplifying assumptions:

- Single-phase, incompressible flow with uniform and constant fluid density and viscosity (no phase changes). As a result, there is no cross-flow between layers.
- Areal homogeneity within a layer
- Uniform layer width in the third (y) dimension.
- On the pore scale, local thermal equilibrium, i.e. immediate thermal equilibration between fluid and surrounding rock grains.
- Perfectly insulated top and bottom boundaries.

(1) Dimensionless variables.

To facilitate the problem description, we deploy dimensionless variables:

$$\left.\begin{aligned} T_D &= \frac{T_{inj} - T}{T_{inj} - T_{ini}} \\ x_D &= \frac{x}{L} \\ z_D &= \frac{z}{H} \\ Q_D &= \frac{\bar{v}t}{L} \end{aligned}\right\}, \tag{1}$$

where T_D is the dimensionless temperature with temperature T normalized with respect to injection (T_{inj}) and initial (T_{ini}) temperatures; x_D and z_D are the dimensionless horizontal and vertical positions, with coordinates x and z normalized by reservoir length L and total thickness H, respectively; Q_D is the dimensionless time, representing the total heat capacity of the fluid volume injected at time t divided by the heat capacity of the two-layer medium. $\bar{v}$ in Q_D is the average velocity of the cooling-front in the two-layer system, which is given below.

(2) Cooling-front velocity

The volumetric heat capacity of layer j is the volume-weighted average of water ($\rho_w c_{pw}$) and rock grain ($\rho_{gj} c_{pgj}$) heat capacities:

$$(\rho c_p)_j = \varphi_j \rho_w c_{pw} + (1 - \varphi_j)\rho_{gj} c_{pgj}. \tag{2}$$

The average heat capacity of the two-layer system is the thickness-weighted average:

$$\overline{(\rho c_p)} = \frac{(\rho c_p)_1 h_1 + (\rho c_p)_2 h_2}{H}. \tag{3}$$

Assuming local thermal equilibrium (i.e. instantaneous thermal equilibration between fluid and rock grains through which it flows) and no dispersion between cold and hot regions within layers or conduction between layers, T_D at the cooling front is a unit step change in each layer. We define a control volume of dimensions ($Wh_j\Delta x$) just ahead of the cooling front, where W is the reservoir width in the y direction. The front advances through this volume in time Δt. An energy balance on this volume gives the velocity of the cooling front in each layer j:

$$v_j = \frac{\Delta x}{\Delta t} = \frac{u_j \rho_w c_{pw}}{\varphi_j \rho_w c_{pw} + (1 - \varphi_j)\rho_{gj} c_{pgj}} = \frac{u_j \rho_w c_{pw}}{(\rho c_p)_j}, \tag{4}$$

where u_j is the Darcy velocity in layer j.

The pore velocity of fluid is (u_j/ϕ_j). v_j in Eq. 4 is proportional to the fluid pore velocity (u_j/ϕ_j), but slowed down by a heat-capacity ratio of

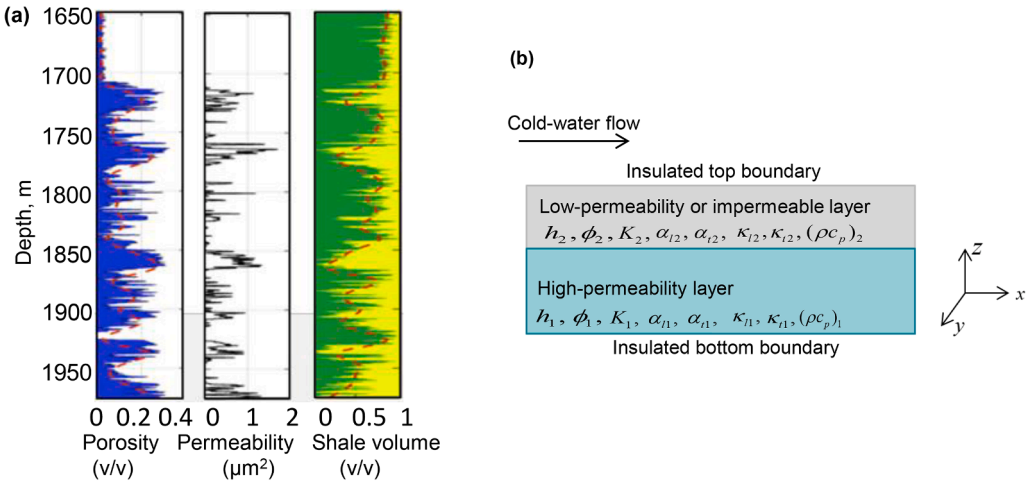

Fig. 2. Geothermal formations featuring interspersed layers: **(a)** well-log data (Bredesen et al., 2020) and **(b)** a two-layer model.

the fluid to fluid-matrix combination, $[(\rho_w c_{pw})\phi_j/(\rho c_p)_j]$. This delay is known as the retardation effect (Oldenburg and Pruess, 1998).

Assuming instantaneous thermal equilibration across the layers and no dispersion in the flow (x) direction gives the thermal-front velocity, $\bar{v}$, i.e. heat capacity-thickness weighted average:

$$\bar{v} = \frac{\Delta x}{\Delta t} = \frac{u_1\rho_w c_{pw}h_1 + u_2\rho_w c_{pw}h_2}{\left[\varphi_1\rho_w c_{pw} + (1-\varphi_1)\rho_{g_1}c_{pg1}\right]h_1 + \left[\varphi_2\rho_w c_{pw} + (1-\varphi_2)\rho_{g_2}c_{pg2}\right]h_2} = \frac{v_1(\rho c_p)_1 h_1 + v_2(\rho c_p)_2 h_2}{(\rho c_p)_1 h_1 + (\rho c_p)_2 h_2}. \tag{5}$$

The heterogeneity of the system in Fig. 2b is characterized by the following factors:

$F_h \equiv \frac{h_1}{H}$: Fraction of total thickness in the high-permeability layer

$F_c \equiv \frac{(\rho c_p)_1}{(\rho c_p)_2}$: Heat-capacity contrast between layers

$F_{ch} \equiv \frac{(\rho c_p)_1 h_1}{(\rho c_p)_2 h_2}$: Heat capacity-thickness contrast between layers

$F_K \equiv \frac{K_1}{K_2}$: Permeability contrast between layers

For the scenario with two permeable layers, Eqs. 4 and 5, incorporating Darcy's Law for u_j, yields the following velocity correlations:

$$\left.\begin{aligned} \frac{v_1}{v_2} &= \frac{F_K}{F_c} \\ \frac{v_1}{\bar{v}} &= \frac{(F_{ch}+1)F_K}{F_K F_{ch} + F_c} \\ \frac{v_2}{\bar{v}} &= \frac{(F_{ch}+1)F_c}{F_K F_{ch} + F_c} \end{aligned}\right\}. \tag{6}$$

Eqs. 2 and 3 give the heat-capacity relations:

$$\left.\begin{aligned} \frac{(\rho c_p)_1}{(\overline{\rho c_p})} &= \frac{F_c}{F_c F_h + (1-F_h)} \\ \frac{(\rho c_p)_2}{(\overline{\rho c_p})} &= \frac{1}{F_c F_h + (1-F_h)} \end{aligned}\right\}. \tag{7}$$

For the scenario with one layer impermeable, i.e. $K_2 = 0$, the heat-capacity relations in Eq. 7 still hold. Nevertheless, as $v_2 = 0$, the velocity relations in Eq. 6 become

$$\left.\begin{aligned} \frac{v_1}{\bar{v}} &= \frac{F_{ch}+1}{F_{ch}} \\ \frac{v_2}{\bar{v}} &= 0 \end{aligned}\right\}. \tag{8}$$

3. Definition of transverse thermal-conduction number N_{TC}

The thermal lifetime of a geothermal process is usually dominated by pressure-driven convection. Nevertheless, it is strongly affected by thermal conduction, in particular conduction in the transverse direction arising from nonuniform cooling fronts between the layers. The transverse conduction slows down the advance of the convection-driven cooling fronts, elongating the breakthrough time of cold water and thus thermal lifetime. As a measure of the transverse thermal conduction relative to convection, we define a dimensionless number N_{TC}, a time ratio given by

$$N_{TC} \equiv \frac{t_{lj}}{t_{tj}} = \frac{L}{H}\frac{e_{tj}}{e_{lj}}, \tag{9}$$

where

t_{lj}: convection-driven thermal-front breakthrough time in layer j;

t_{tj}: transverse thermal-conduction time across the two layers;

(e_{tj}/e_{lj}): ratio of heat fluxes driven by transverse conduction and longitudinal convection:

$$e_{lj} = v_j T_D, \tag{10}$$

$$e_{tj} = -\left(\frac{\alpha_{tj}}{H}\right)\cdot\left(\frac{\Delta T_D}{\Delta z_D}\right). \tag{11}$$

Substituting Eqs. 10 and 11 into Eq. 9 yields

$$N_{TC} = \frac{L}{H^2}\frac{\alpha_{tj}}{v_j}\left(\frac{-\Delta T_D/\Delta z_D}{T_D}\right). \tag{12}$$

Following Lake and Hirasaki (1981), we take $[(-\Delta T_D/\Delta z_D)/T_D]$ in Eq. 12 to be a constant, 12.5, and choose properties making N_{TC} minimum. N_{TC} is the minimum of the following two expressions:

$$\begin{aligned} N_{TC} &= 12.5 \times \frac{L}{H^2}\frac{\alpha_{t2}}{v_1}, \qquad or \\ &= 12.5 \times \frac{L}{H^2}\frac{\alpha_{t1}}{v_1}. \end{aligned} \tag{13}$$

The reason for the choice of the factor 12.5 is given below in the verification of the definition of N_{TC}; compare the 12.5 in Eq. 13 for heat conduction with Eqs. 14 in Lake and Hirasaki and 14.44 in Taylor (1953) for solute transport. The verification of the factor 12.5 in the definition of N_{TC} given below is based on cases with a wide variety of layer geometries with the same initial and injection temperatures. It is possible that an application with a very-different ratio of absolute temperatures might require an adjustment of this value. Greater values of N_{TC} mean either slower convection or faster conduction. Both suggest a larger proportion of the system is at transverse thermal equilibrium during cold-water injection.

4. Derivation of effective longitudinal thermal diffusivity - α_{eff}

The detailed derivation of the effective longitudinal thermal diffusivity, α_{eff}, is shown below for the scenario with two layers, both permeable. The scenario with an impermeable layer follows the same procedures.

With the assumptions in the Section 2.2, the energy-balance equation for an infinitesimal volume element in the 2D system of Fig. 2b is

$$\frac{\partial T}{\partial t} + v_j\frac{\partial T}{\partial x} - \alpha_{lj}\frac{\partial^2 T}{\partial x^2} - \alpha_{tj}\frac{\partial^2 T}{\partial z^2} = 0, \tag{14}$$

where j denotes layer 1 or 2. v_j is given in Eq. 4, which varies in cross-section as a function of layer index j, i.e. the cause for thermal Taylor dispersion. We transform x to dimensionless coordinate $\hat{x}_D$:

$$\hat{x}_D = \frac{x}{L} - \frac{\bar{v}t}{L} = x_D - Q_D, \tag{15}$$

which is the position relative to a vertical plane moving at velocity $\bar{v}$.

When transverse thermal conduction is significant, i.e. at large values of N_{TC}, the cooling front spreads slowly around the position $(\bar{v}t)$ (e.g., Taylor (1953)). This suggests that in the equation recast in terms of $\hat{x}_D$, the term $(\partial T/\partial t)$ in Eq. 14 is small and can be neglected: conduction/dispersion around the front spreads like the square root of time and slows down with time. Following Taylor's result and implications of previous work on dispersion in heterogeneous media, we leave out axial heat conduction for simplicity. This simplification gives an equivalent diffusion coefficient representing non-uniform convection and transverse conduction between layers. Eq. 14, inserting dimensionless variables $\hat{x}_D$ and z_D, then becomes:

$$\left(\frac{v_j}{\bar{v}} - 1\right)\frac{\partial T_D}{\partial \hat{x}_D} = \left(\frac{L}{H}\right)^2\frac{\partial}{\partial z_D}\left(\frac{\alpha_{tj}}{\bar{v}L}\frac{\partial T_D}{\partial z_D}\right). \tag{16}$$

Hereafter, the term $(\partial T_D/\partial \hat{x}_D)$ is treated as independent of z_D; this treatment is justified by the fact that significant transverse conduction almost equalizes temperature in the z direction at position $\hat{x}_D$. At boundaries $z_D = 0$ and 1, heat flux is zero. We integrate both sides of Eq. 16 with respect to z_D, over $[0, z_D]$ for $0 \le z_D < F_h$ (layer $j = 1$) and over $[z_D, 1]$ for $F_h \le z_D \le 1$ (layer $j = 2$), respectively. Performing a second integration, over $[0, z_D]$ for $0 \le z_D < F_h$ and over $[F_h, z_D]$ for $F_h \le z_D \le 1$, yields the transverse T_D profile as a function of z_D:

for $0 \le z_D < F_h$:

$$T_D = T_D|_{z_D=0} + \frac{1}{2}\left(\frac{\overline{\nu}L}{\alpha_{t1}}\right)\left(\frac{H}{L}\right)^2\left(\frac{\nu_1}{\overline{\nu}} - 1\right)\left(z_D^2\right)\left(\frac{\partial T_D}{\partial \hat{x}_D}\right), \tag{17}$$

for $F_h \le z_D \le 1$:

$$\begin{aligned} T_D \;&= T_D|_{z_D=0} + \frac{1}{2}\left(\frac{\overline{\nu}L}{\alpha_{t1}}\right)\left(\frac{H}{L}\right)^2\left(\frac{\nu_1}{\overline{\nu}} - 1\right)\left(F_h^2\right)\left(\frac{\partial T_D}{\partial \hat{x}_D}\right) \\ &+ \frac{1}{2}\left(\frac{\overline{\nu}L}{\alpha_{t2}}\right)\left(\frac{H}{L}\right)^2\left(\frac{\nu_2}{\overline{\nu}} - 1\right)\left(z_D^2 - 2z_D - F_h^2 + 2F_h\right)\left(\frac{\partial T_D}{\partial \hat{x}_D}\right), \end{aligned} \tag{18}$$

where T_D in Eqs. 17 and 18 is equal at $z_D = F_h$, maintaining a continuous heat flux across the layer boundary.

Based on the transverse T_D (z_D) profile, one can solve for the convective heat flux, e_c across the moving plane at $\overline{\nu}t$, through the following integration:

$$\begin{aligned} e_c \;&= WH\int_0^1 (\nu_j - \overline{\nu})(\rho c_p)_j T_D dz_D \\ &= WH\int_0^{F_h} (\nu_1 - \overline{\nu})(\rho c_p)_1 T_D dz_D + WH\int_{F_h}^1 (\nu_2 - \overline{\nu})(\rho c_p)_2 T_D dz_D. \end{aligned} \tag{19}$$

e_c is determined by substituting T_D in Eqs. 17 and 18 into the corresponding integral in Eq. 19. With the relations in Eqs. 6 and 7, the expression for e_c is derived as follows:

$$\begin{aligned} e_c = -\frac{WH\overline{\nu}(\overline{\rho c_p})}{3}\left(\frac{H}{L}\right)^2\left(\frac{F_c F_h}{F_c F_h + 1 - F_h}\right)\left(\frac{F_K - F_c}{F_K F_{ch} + F_c}\right)^2\left[\left(\frac{\overline{\nu}L}{\alpha_{t1}}\right)F_h^2\right. \\ \left. + \left(\frac{\overline{\nu}L}{\alpha_{t2}}\right)F_c F_h(1 - F_h)\right]\left(\frac{\partial T_D}{\partial \hat{x}_D}\right) + \omega, \end{aligned} \tag{20}$$

where ω is a collection of terms independent of $\hat{x}_D$ and canceled in the derivative of e_c to $\hat{x}_D$ below.

Within the front of dimension $(WHd\hat{x}_D)$, an energy balance over time interval dQ_D yields

$$WH\overline{\nu}(\overline{\rho c_p})\frac{\partial \widetilde{T}_D}{\partial Q_D} + \frac{\partial e_c}{\partial \hat{x}_D} = 0, \tag{21}$$

where $\widetilde{T}_D$ is the average temperature in cross-section at $\hat{x}_D$, which is approximately T_D when thermal equilibration across z_D is nearly instantaneous (i.e. at large values of N_{TC}). Solving for the derivative of e_c in Eq. 20 with respect to $\hat{x}_D$ and substituting the derivative into Eq. 21 yields

$$\frac{\partial T_D}{\partial Q_D} = (N_{pe})^{-1}\frac{\partial^2 T_D}{\partial \hat{x}_D^2}, \tag{22}$$

where $(N_{pe})^{-1}$ is the equivalent inverse Péclet number as contributed by Taylor dispersion:

$$(N_{pe})^{-1} = \frac{\overline{\nu}H^2}{3L}\left(\frac{F_c F_h}{F_c F_h + 1 - F_h}\right)\left(\frac{F_K - F_c}{F_K F_{ch} + F_c}\right)^2\left[\frac{F_h^2}{\alpha_{t1}} + \frac{F_c F_h(1 - F_h)}{\alpha_{t2}}\right]. \tag{23}$$

The effective longitudinal diffusivity, α_{eff} is the sum of longitudinal diffusivity and extra diffusivity resulting from heterogeneous convection modified by transverse conduction, analogous to solute dispersion (Aris, 1956; Lake and Hirasaki, 1981):

$$\alpha_{eff} = \overline{\alpha}_l + \overline{\nu}L(N_{pe})^{-1}, \tag{24}$$

where $\overline{\alpha}_l$ is the thickness-weighted average of α_{l1} and α_{l2}.

Combining Eqs. 23 and 24 yields the analytical model for α_{eff} for the scenario with two permeable layers:

$$\alpha_{eff} = \overline{\alpha}_l + \frac{\overline{\nu}^2 H^2}{3}\left(\frac{F_c F_h}{F_c F_h + 1 - F_h}\right)\left(\frac{F_K - F_c}{F_K F_{ch} + F_c}\right)^2\left[\frac{F_h^2}{\alpha_{t1}} + \frac{F_c F_h(1 - F_h)}{\alpha_{t2}}\right], \tag{25}$$

where α_{eff} has the units of m^2/s, when the parameters in the equation use standard units. Note that α_{eff} here and in Eq. 26 below is an effective thermal diffusivity accounting for both water and rock. Treating α_{eff} as volume-weighted average of diffusivities of water and rock, one can then calculate back the effective diffusivity of rock from α_{eff}.

For the scenario with an impermeable layer, the derivation of α_{eff} follows the same steps from Eqs. 14 to 25. To account for K_2 being zero, the relations in Eq. 8 should be used in deriving e_c in Eq. 20. The corresponding expression for α_{eff} in this scenario then becomes:

$$\alpha_{eff} = \overline{\alpha}_l + \frac{\overline{\nu}^2 H^2}{3}\left(\frac{F_c F_h}{F_c F_h + 1 - F_h}\right)\left(\frac{1}{F_{ch}}\right)^2\left[\frac{F_h^2}{\alpha_{t1}} + \frac{F_c F_h(1 - F_h)}{\alpha_{t2}}\right]. \tag{26}$$

Eq. 25 or 26 multiplied by $(\overline{\rho c_p})$ in Eq. 3 gives the effective longitudinal thermal conductivity, κ_{eff}. Similar to α_{eff}, κ_{eff} in the flow direction is the sum of longitudinal conductivity (i.e. thickness-weighted average of κ_{l1} and κ_{l2}) and extra conductivity resulting from nonuniform convection and transverse conduction. The effective conductivity of rocks can be calculated from κ_{eff}, when treated as volume-weighted average of the conductivities of water and rock.

5. Verification of the N_{TC} and α_{eff} Model

We verify both the N_{TC} and α_{eff} equations via comparison with 2D numerical solutions of Eq. 14 for $T(x, z, t)$. Simulation results were obtained with DARTS (Delft Advanced Research Terra Simulator) for geothermal processes (see Khait and Voskov (2018) and Wang et al. (2020) for details of the simulator). The mass- and energy-balance equations were numerically solved in a fully implicit manner using the same inputs as in the analytical model. In the setup of the numerical model, the reservoir was initially saturated with single-phase water at 80 °C and 190 bar. At the injection-well boundary, cold-water of 30 °C was injected at a fixed rate, with whole thickness of the reservoir perforated. There is no flux across other boundaries, except at production well, which is perforated all along its length. The assumption of incompressibility and no density change with temperature for both fluid and rock assures that the fluid velocities are identical in the analytical and numerical modeling. The reservoir length is 1000 m and width 1 m. In our simulation runs, grid resolution (1 × 1 × 1 m) and a time step of maximum 10 days were utilized to represent actual thermal dispersion with minimized numerical diffusion.

Table 1 lists the layer properties of the media used for illustrations of analytical and numerical modeling. We assume all properties are isotropic within a layer. The values of permeability and porosity refer to a geothermal reservoir in Copenhagen, Denmark (Bredesen et al., 2020). In the field example of Bredesen et al., permeable and impermeable layers are sandstone and shale, respectively. The thermophysical properties for sandstone and shale are taken from Lake et al. (2014). Heat capacity, $(\rho c_p)_j$ of layer j is the volume-weighted average of the heat capacities of water and rock grains, as given in Eq. 2 in Section 2.2. Similarly, original thermal conductivity κ_j and diffusivity α_j assigned to each layer j are the volume-weighted averages of the corresponding thermophysical properties of water and rock grains.

Table 2 summarizes the simulation results. The operation rates in geothermal fields vary greatly due to different formation properties, production rates and project lifespans. The tested injection rates (in

Table 1
Layer properties used for illustrating the validity of N_{TC} and α_{eff} model.

Layer 1 properties					Layer 2 properties					Water
ϕ_1	K_1, m^2	$(\rho c_p)_1$, KJ/m^3.K	κ_1, W/m.k	α_1, m^2/s	ϕ_2	K_2, m^2	$(\rho c_p)_2$, KJ/m^3.K	κ_2, W/m.K	α_2, m^2/s	$(\rho c_p)_w$, KJ/m^3.K
0.19	5×10^{-13}	2267.73	2.61	1.15×10^{-6}	0.19	1.25×10^{-13}	2267.73	2.61	1.15×10^{-6}	4190
0.19	5×10^{-13}	2267.73	2.61	1.15×10^{-6}	0	0	1754.19	1.61	0.92×10^{-6}	4190

Table 2
Numerical simulation results for transverse thermal conduction.

Cases*	h_1, m	h_2, m	Q, m^3/D	dp, bar	κ_{eff}, W/(m.K)	α_{eff}, m^2/s	N_{TC}	$(Q_{D0})_{TD=0.5}$	$(Q_D)_{TD=0.5}$	I_{TC}
1	10	2	0.8496	15.03	5.68	2.51×10^{-6}	57.74	0.875	1.000	1.000
2	10	2	0.4252	7.91	3.52	1.61×10^{-6}	87.61	0.866	1.000	1.000
3	10	5	0.5315	9.88	10.23	4.89×10^{-6}	44.86	0.721	1.000	1.000
4	10	10	0.7087	13.16	39.72	1.98×10^{-5}	18.92	0.564	1.001	1.002
5	10	20	1.0631	19.60	179.02	9.30×10^{-5}	5.61	0.393	0.944	0.908
6	10	30	1.4174	25.62	433.86	2.30×10^{-4}	2.37	0.301	0.835	0.763
7	10	40	1.7718	31.33	807.92	4.35×10^{-4}	1.21	0.244	0.659	0.549
8	10	50	2.1261	36.99	1302.61	7.08×10^{-4}	0.70	0.205	0.499	0.370
9	10	90	3.5435	60.92	4497.16	2.49×10^{-3}	0.15	0.126	0.232	0.122

* In each case, $T_{inj} = 30$ °C and $T_{ini} = 80$ °C, and simulations of Case 1 and Cases 2 – 9 use the first and second row of layer properties in Table 1, respectively. *dp* denotes the overall pressure drop.

Table 2) scale up with reservoir thickness and are within the range of field rates, e.g. 0.7 to 4 m^3/D over a cross-section area of 100 m^2 (e.g. Bujakowski et al., 2016; Feng et al., 2017; Wang et al., 2021). Table 2 also lists the upscaled thermal conductivity and diffusivity values, which can be much greater than those of the rock itself. For instance, in Case 5, κ_{eff} = 179.02 W/(m.K), nearly 69 times the conductivity of water-sandstone mixture, 2.61 W/(m.k); $\alpha_{eff} = 9.30 \times 10^{-5}$ m^2/s, nearly 81 times the thermal diffusivity of the water-sandstone mixture, 1.15×10^{-6} m^2/s. In conventional upscaling without accounting for Taylor dispersion, the upscaled thermo-physical properties are much less than we show here, e.g. close to those of the rocks involved. Due to underestimated thermal conductivity/diffusivity in conventional upscaling, thermal dispersion is underestimated, which would result in overestimation of thermal breakthrough time.

5.1. Verification of the transverse thermal-conduction number N_{TC}

To verify the definition of N_{TC} in Eq. 13, a transverse thermal-conduction index is introduced:

$$I_{TC} \equiv \frac{(Q_D)_{T_D=0.5} - (Q_{D0})_{T_D=0.5}}{1 - (Q_{D0})_{T_D=0.5}}, \tag{27}$$

where $(Q_D)_{TD=0.5}$ and $(Q_{D0})_{TD=0.5}$ (given in Eq. 1) represent the cumulative heat injection at the breakthrough of $T_D = 0.5$, with and without thermal conduction in either direction, respectively. $T_D = 0.5$ is chosen as a representation of the cooling-front breakthrough. In the calculations of I_{TC}, $(Q_D)_{TD=0.5}$ (in Eq. 1) is obtained from simulations of various cases in Table 2. $(Q_{D0})_{TD=0.5}$ depends on F_{Kh}. For a system with two permeable layers, it is given by

$$\begin{cases} For\ F_{Kh} > 1 & (Q_{D0})_{T_D=0.5} = \dfrac{F_K F_{ch} + F_c}{(F_{ch}+1)F_K} \\ For\ F_{Kh} < 1 & (Q_{D0})_{T_D=0.5} = \dfrac{F_K F_{ch} + F_c}{(F_{ch}+1)F_c} \end{cases}. \tag{28}$$

For a system with an impermeable layer, F_{Kh} is always greater than unity and $(Q_{D0})_{TD=0.5}$ is

$$(Q_{D0})_{T_D=0.5} = \frac{F_{ch}}{F_{ch}+1}. \tag{29}$$

The value of I_{TC} in Eq. 27 indicates the accuracy of the assumption of instantaneous transverse thermal-equilibration across the two layers, as the cooling front advances. $I_{TC} = 1$ indicates approximately instantaneous thermal equilibration and $I_{TC} = 0$ indicates least thermal equilibration across the two layers. For $I_{TC} = 1$, $(Q_D)_{TD=0.5} = 1$, meaning that the heat injection required is the heat capacity of the whole system at the breakthrough of $T_D = 0.5$. This occurs only when transverse thermal equilibration is approximately instantaneous. For $I_{TC} = 0$, $(Q_D)_{TD=0.5} = (Q_{D0})_{TD=0.5}$, meaning that the heat injection required is that as though with no transverse conduction at all.

The behavior of I_{TC} is illustrated by the 2D T distribution with respect to different values of I_{TC}, as shown in Fig. 3. For instance, in Case 2 with top impermeable layer of $h_2 = 2$ m and bottom permeable layer of $h_1 = 10$ m, $I_{TC} = 1$ and uniform T in the cross-section reflects instantaneous or fast equilibration across the layers. With the thickness of the impermeable layer h_2 increasing, e.g. $h_2 = 20$ m in Case 5 and $h_2 = 90$ m in Case 9 where I_{TC} = 0.908 and 0.122, transverse heat conduction is not fast enough to achieve uniform T in the cross-section.

Fig. 4 shows a good correlation between N_{TC} in Eq. 13 and I_{TC} in Eq. 27. For illustration, nine simulations were conducted with respect to different thickness contrasts between the low-permeability or impermeable layer (h_2) and high-permeability layer (h_1), as summarized in Table 2. Each simulation run gives a value of I_{TC}, and, based on the layer properties, one can calculate the corresponding value of N_{TC}. With h_2 (the low-permeability layer) increasing relative to h_1 (the high-permeability layer), N_{TC} decreases from 87.61 to 0.15. Also, it takes longer for transverse conduction across the two layers, meaning a smaller fraction of the system at transverse thermal equilibration (Fig. 3). Less vertical thermal equilibration corresponds to I_{TC} decreasing from 1 towards 0. The consistency between N_{TC} and I_{TC} suggests that N_{TC} can be used as an indicator of transverse thermal equilibration without running simulations.

The constant 12.5 included in the definition of N_{TC} in Eq. 13 is chosen such that $N_{TC} = 1$ at $I_{TC} = 0.5$, for convenience. For $N_{TC} < 0.01$, I_{TC} is about 0, indicating that a two-layer medium behaves like two layers with no thermal interaction between the layers. For $N_{TC} > 5$, $I_{TC} > 0.88$: the two layers are approaching transverse thermal equilibrium, as shown in Cases 2 and 5 of Fig. 3. This further implies, for $N_{TC} > 5$, that thermal dispersion in a two-layer system approximates a single homogeneous layer. Therefore, $N_{TC} > 5$ defines a physical criterion for combining two layers. In addition, the α_{eff} model in Eq. 25 or 26 is derived assuming instantaneous thermal equilibration in the cross-section, so $N_{TC} > 5$ also defines the valid condition for the α_{eff} model. As illustrated in Case 9 of Fig. 3, with $N_{TC} < 5$, a two-layer medium exhibits heterogeneous behavior in the T distribution, violating the α_{eff}

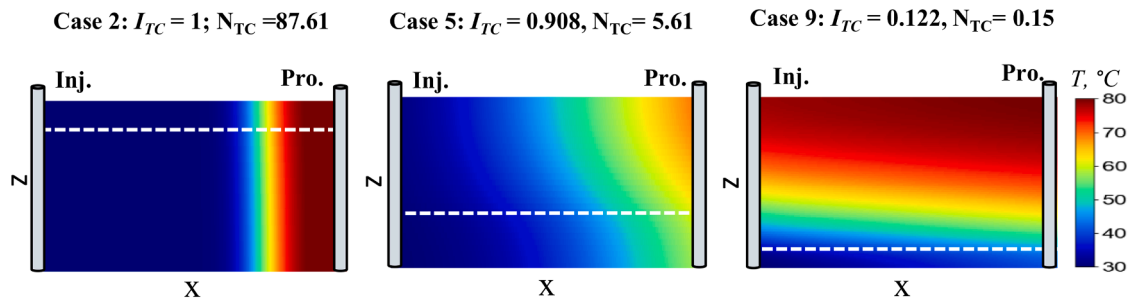

Fig. 3. 2D temperature (T) distribution at 30 years of cold-water injection in Cases 2, 5 and 9. Dashed line marks layer boundary, with the higher-permeability layer at the bottom in each case. In each case, the injection and production wells are perforated through the entire thickness of the formation.

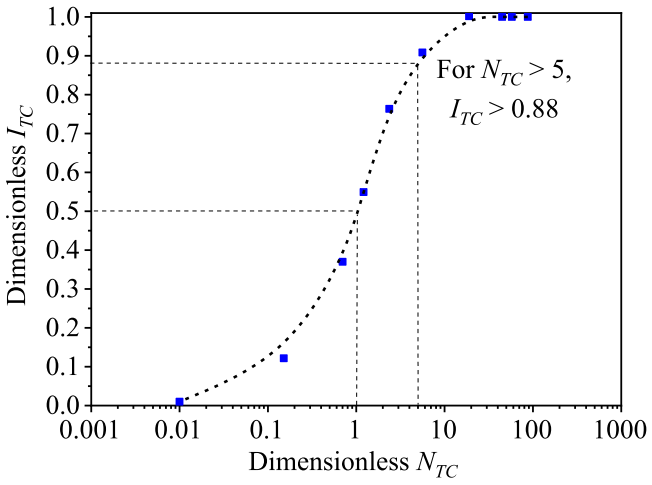

Fig. 4. Verification of the transverse thermal-conduction number, N_{TC} (Eq. 13) as an indicator for transverse thermal equilibration in vertical cross-section.

model's assumption of instantaneous thermal equilibration. Thus, for $N_{TC} < 5$, a two-layer medium should not be combined in terms of thermal dispersion. The N_{TC} criterion and α_{eff} model is further verified in the next section.

5.2. Verification of the effective longitudinal thermal-diffusivity model α_{eff}

Eq. 22 represents the energy-balance equation for a single-layer medium having the average properties of the two-layer system in Fig. 2b. Replacing $(N_{pe})^{-1}$ with the effective inverse Péclet number $(N_{pe}^{eff})^{-1}$, an approximate solution to Eq. 22 follows an error function (Murphy et al., 1981; Axelsson et al., 2005):

$$T_D = 1 - \frac{1}{2}\left[1 - erf\left(\frac{x_D - Q_D}{2\sqrt{Q_D\left(N_{pe}^{eff}\right)^{-1}}}\right)\right], \tag{30}$$

where

$$\left(N_{pe}^{eff}\right)^{-1} \equiv \frac{\alpha_{eff}}{\bar{v}L}. \tag{31}$$

Using Eqs. 30 and 31 and layer properties in Table 1, one can solve analytically for $T(x, t)$ for the combined single-layer medium possessing the average properties of the two layers.

Fig. 5 compares the analytical solutions with numerical solutions for both produced T history and T distribution along x, with respect to N_{TC} values. In the numerical solutions, the produced T history reported on the left column is a volumetric-flow-rate-weighted average of produced T from the last column of grid blocks. The T profile reported on the right column in Fig. 5 is a volume-weighted average of T in the vertical column of grid blocks at each position x_D.

In the analytical solutions, α_{eff} in Eq. 25 or 26 is used to represent the effective longitudinal thermal diffusivity in the combined system. For $N_{TC} > 5$, e.g. $N_{TC} = 57.74$ in Case 1 and 5.61 in Case 5, a good match between analytical and numerical solutions is achieved in both effluent T history and T profile. The good match verifies the effectiveness of the α_{eff} model for representing thermal Taylor dispersion in a two-layer system, when satisfying the criterion $N_{TC} > 5$. For $N_{TC} < 5$, e.g. $N_{TC} = 1.21$ in Figs. 5e and 5f from Case 7, the fit is not as good. The deviation means that the α_{eff} does not represent the effective thermal dispersion at low values of N_{TC}. This is because low values of N_{TC} correspond to slow transverse thermal conduction relative to convection. As a result, transverse thermal conduction is not fast enough to give a uniform T in the vertical cross-section. Thus, the two layers should not be combined into a single layer or represented by α_{eff} for $N_{TC} < 5$.

5.3. Application of the model to upscaling well-log data of a geothermal reservoir

The concept of effective thermal dispersion can be applied to upscaling the modeling of various subsurface thermal processes, e.g. geothermal and thermal enhanced oil recovery processes. There would also be similarities to dispersion of gas fronts in hydrogen-storage applications, in that the magnitude of gas diffusion coefficients is similar to that of thermal conductivity, though the details of the derivation differ (Lake and Hirasaki, 1981). This suggests that in both applications, upscaling is feasible to a greater extent than with dispersion in liquid flow.

Conventional upscaling approaches use arithmetic or volumetric averaging to estimate dispersion coefficients in layers combined in a simulation grid block. Such averaging does not account for the non-uniform convection modified by transverse conduction between the layers within a grid block. This underestimates the spreading of dispersion fronts, leading to overestimation of the time to thermal breakthrough (e.g. Babaei and Nick, 2019; Daniilidis et al., 2020). The analytical model α_{eff} accounting for thermal Taylor dispersion provides a more-accurate representation of thermal dispersion in an upscaled system. Below we outline the general approach for extending the N_{TC} layer-combining criterion and α_{eff} model to multi-layer media.

For a multi-layer medium as in Fig. 6a, one can upscale thermal conductivities with the α_{eff} model by combining layers in stages (two layers per stage). Here we outline the procedures for upscaling a formation with n layers. One starts with calculating the values of N_{TC} (Eq. 13) for each pair of adjacent layers, e.g. N_{TC} for layers 1 and 2, layers 2 and 3, …, layers (n-1) and n. Then, the two layers with maximum N_{TC} (when satisfying the upscaling criterion $N_{TC} > 5$) are combined into one layer represented by average properties. In particular, in the combined-group permeability is upscaled by thickness-weighted average and thermal conductivity in the flow direction is calculated with the upscaling model in Eq. 25 or 26. The n-layer system now forms a new

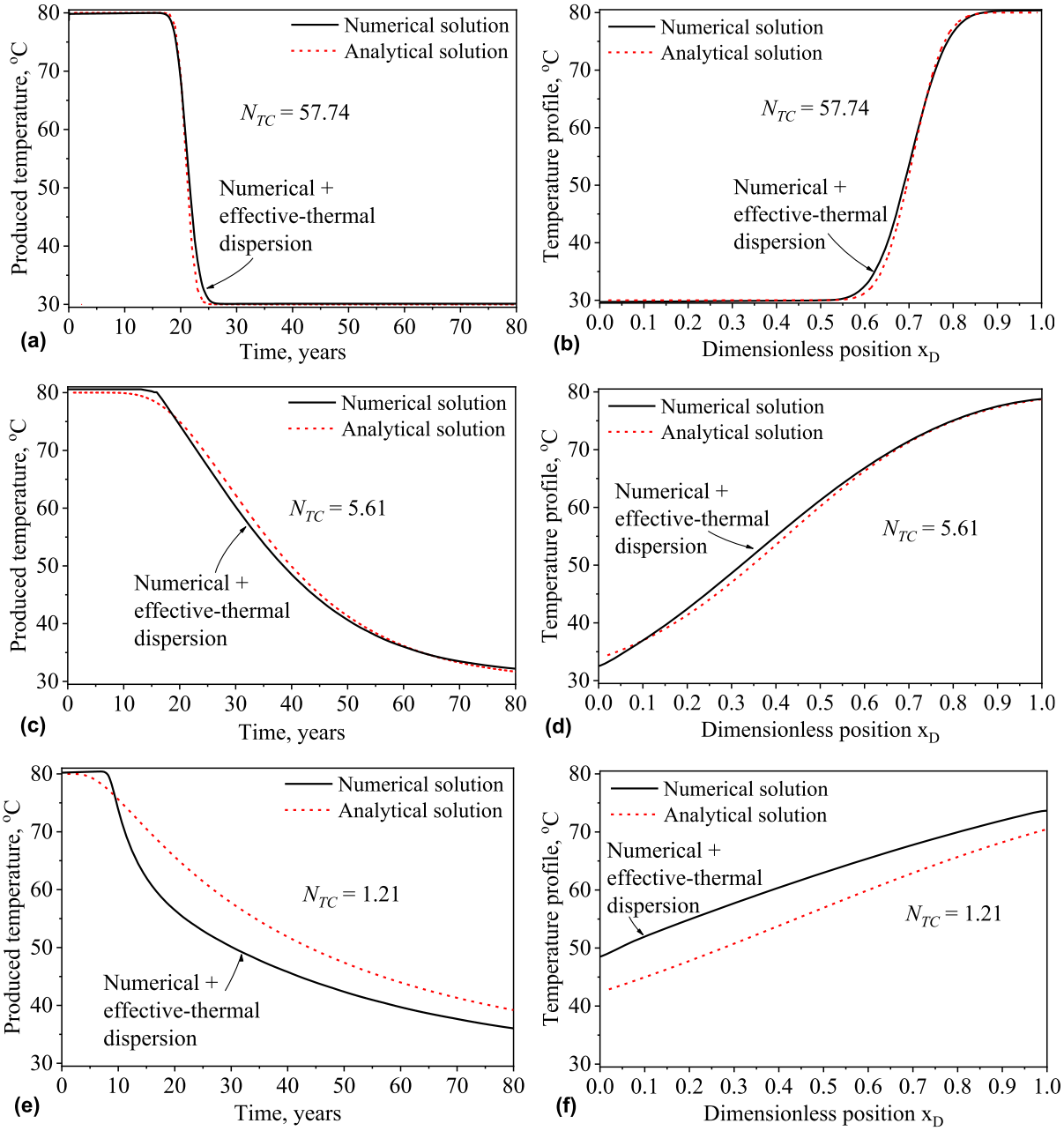

Fig. 5. Verification of the α_{eff} model (Eqs. 25 and 26) via comparison with numerical solutions for effluent T history and T profile (at 15 years): **(a)** and **(b)** from Case 1; **(c)** and **(d)** from Case 5; **(e)** and **(f)** from Case 7. See Tables 1 and 2 for detailed simulation inputs.

system with (n-1) layers after the first stage of upscaling. With the combined system, one calculates again the values of N_{TC}, combines the two layers with maximum N_{TC} and calculates the average properties in the combined group as above. This process proceeds until no more adjacent layers satisfy the upscaling criterion.

An application example of upscaling the well-log data of a geothermal reservoir is given in Fig. 6. With multi-stage upscaling, a 91-layer geothermal reservoir is combined to 12 layers. Again, the upscaled thermal conductivities accounting for the fine-scale heterogeneity in the combined layers, as shown in Fig. 6c, are much greater than those obtained with conventional upscaling methods by averaging. The upscaled description of the reservoir in Figs. 6b and 6c is then used as inputs for geothermal simulations to enhance the computational efficiency.

The numerical simulation in Fig. 7 uses the formation properties in Fig. 6a, where the grid resolution used represents all 91 layers. This case is conducted as a reference to represent the actual thermal dispersion in the formation. The upscaling simulation in Fig. 7 uses the upscaled properties in Figs. 6b and 6c. The good match between the two verifies the effectiveness of the N_{TC} criterion and α_{eff} model in upscaling the description of stratified geothermal formations.

6. Discussion

For the first time, we develop physically based upscaling criterion (N_{TC}) and upscaling model (α_{eff}) for simplifying characterization of geothermal formations. The α_{eff} model is derived based on simplified assumptions as stated in Section 2.2, to model the basic physics of thermal dispersion in geological formations. Upon the derivation assumptions, the model is applicable to horizontal flow in heterogeneous formations or formations that can be simplified as stratified. Compared with conventional upscaling without considering thermal Taylor dispersion between streamlines, the α_{eff} model represents more

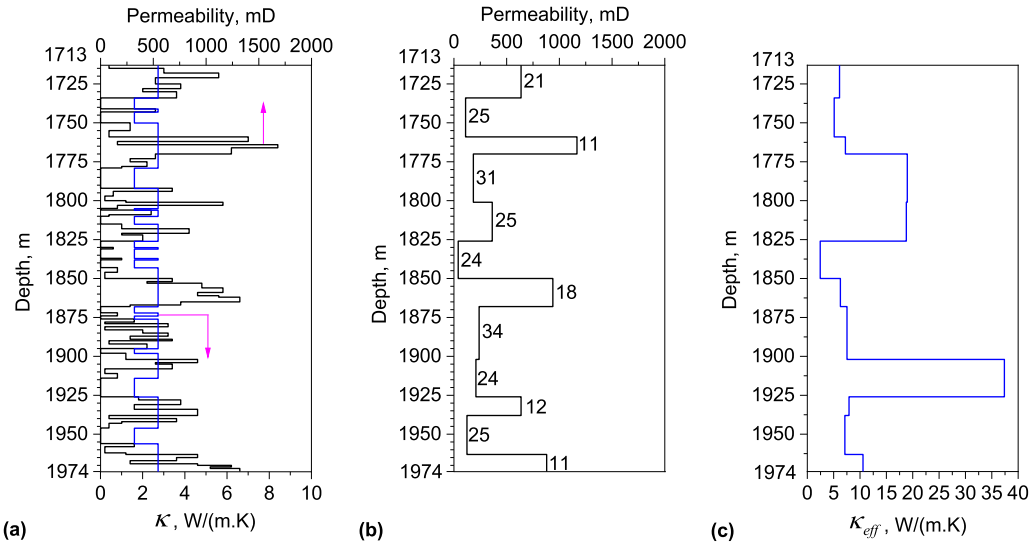

Fig. 6. Upscaling of the well-log data of a geothermal reservoir with 91 layers: (a) original permeability and thermal conductivity; (b) upscaled permeability; (c) upscaled thermal conductivity. Values labelled in Fig. 6b denote the thickness of each upscaled group.

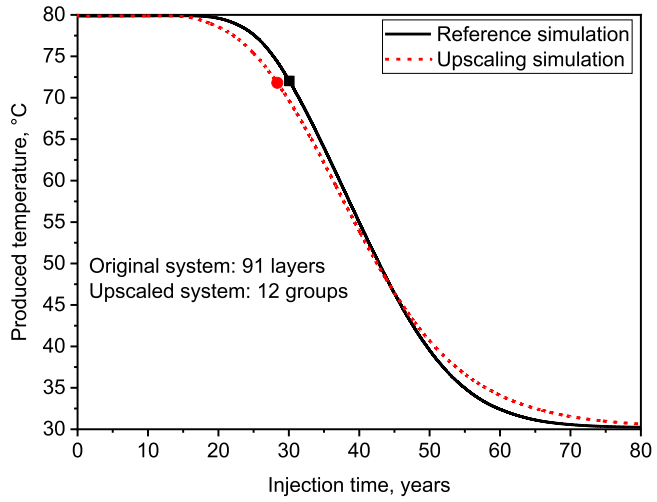

Fig. 7. Comparison in produced-T history between simulations with original (Fig. 6a) and upscaled (Figs. 6b and 6c) formation properties.

accurately the effective thermal dispersion and thus gives more accurate prediction of thermal breakthrough time.

In the field, there are various complex factors, including heat conduction from overburden and underburden formations, areal heterogeneity and fractures, multi-phase flow, gravity effects, etc. These factors have strong impact on thermal dispersion and thus thermal lifetime of a geothermal project. In particular, many geothermal formations are a combination of matrix and fractures. The presence of fractures strongly affects fluid convection and thus thermal dispersion. The extension of our upscaling model to those complex geological formations needs further investigation.

7. Summary and conclusions

Non-uniform fluid velocities combined with heat conduction across streamlines, i.e. thermal Taylor dispersion, mean effective thermal conductivity in the flow direction is greater than that of rock itself. Ignoring this effect, as in conventional upscaling of thermophysical properties, leads to overestimation of thermal breakthrough time of a geothermal doublet.

From an energy balance, we derive an upscaling model, α_{eff}, for effective longitudinal thermal diffusivity, to represent effective thermal dispersion in a two-layer system. α_{eff} accounts for longitudinal heat conduction at the cooling front and transverse heat conduction between streamlines, so it can be much greater than the thermal diffusivity of rock itself.

We define a dimensionless number, N_{TC} (i.e. a ratio of times for longitudinal-convection breakthrough and transverse conduction across the two layers). We find that for $N_{TC} > 5$, a two-layer heterogeneous system can be closely approximated by a single homogenous layer where the effective thermal dispersion can be represented by α_{eff}. Thus, N_{TC} provides a physical criterion for combining two layers.

The N_{TC} criterion and α_{eff} model provides a new physically based upscaling approach to simplify the description of geothermal formations. Its validity is preliminarily verified via an application example of upscaling well-log data of a stratified geothermal formation.

The upscaling criterion and model we present here reveals the basic physics of thermal dispersion in horizontal flow or stratified formations. The extension of the upscaling model to complex geological formations needs further research, e.g. geothermal formations with complexities such as heat conduction from overburden and underburden formations, areal heterogeneity or fractures, multi-phase flow, gravity effects, etc.

CRediT authorship contribution statement

Jinyu Tang: Conceptualization, Formal analysis, Funding acquisition, Investigation, Methodology, Project administration, Resources, Supervision, Validation, Visualization, Writing – original draft, Writing – review & editing. **Yang Wang:** Data curation, Resources, Software, Validation, Visualization. **William R. Rossen:** Conceptualization, Formal analysis, Methodology, Writing – review & editing.

Declaration of competing interest

The authors declare that they have no known competing financial interests or personal relationships that could have appeared to influence the work reported in this paper

Data availability

No data was used for the research described in the article.

Acknowledgments

This project is funded by the United Arab Emirates University Research Grant (Grant No. 12N099) and Natural Science Foundation of Shandong Province (Grant No. ZR2023QE051). The authors acknowledge the insightful discussions and comments by Prof. L. W. Lake of the University of Texas at Austin and Dr. D. Voskov of the Delft University of Technology.

References

Aris, R., 1956. On the dispersion of a solute in a fluid flowing through a tube. Proceedings of the Royal Society of London. Series A. Mathematical and Physical Sciences 235 (1200), 67–77.
Axelsson, G., Björnsson, G., Montalvo, F., 2005. Quantitative interpretation of tracer test data. In: Proceedings World Geothermal Congress, pp. 24–29.
Babaei, M., Nick, H.M., 2019. Performance of low-enthalpy geothermal systems: interplay of spatially correlated heterogeneity and well-doublet spacings. Appl. Energy 253, 113569.
Batycky, R.P., Edwards, D.A., Brenner, H., 1994. Internal energy transport in adiabatic systems: thermal Taylor dispersion phenomena. Int. J. Non Linear Mech. 29 (5), 639–664.
Blank, L., Meneses Rioseco, E., Caiazzo, A., Wilbrandt, U., 2021. Modeling, simulation, and optimization of geothermal energy production from hot sedimentary aquifers. Computat. Geosc. 25 (1), 67–104.
Bredesen, K., Dalgaard, E., Mathiesen, A., Rasmussen, R., Balling, N., 2020. Seismic characterization of geothermal sedimentary reservoirs: a field example from the Copenhagen area, Denmark. Interpretation 8 (2), T275–T291.
Bruderer, C., Bernabé, Y., 2001. Network modeling of dispersion: transition from Taylor dispersion in homogeneous networks to mechanical dispersion in very heterogeneous ones. Water Resour. Res. 37 (4), 897–908.
Bujakowski, W., Tomaszewska, B., Miecznik, M., 2016. The Podhale geothermal reservoir simulation for long-term sustainable production. Renew. Energy 99, 420–430.
Crooijmans, R.A., Willems, C.J., Nick, H.M., Bruhn, D.F., 2016. The influence of facies heterogeneity on the doublet performance in low-enthalpy geothermal sedimentary reservoirs. Geothermics 64, 209–219.
Daniilidis, A., Nick, H.M., Bruhn, D.F., 2020. Interdependencies between physical, design and operational parameters for direct use geothermal heat in faulted hydrothermal reservoirs. Geothermics 86, 101806.
De Bruijn, E.A.M., Bloemendal, M., ter Borgh, M.M., Godderij, R.R.G.G., Vossepoel, F.C., 2021. Quantifying the contribution of heat recharge from confining layers to geothermal resources. Geothermics 93, 102072.
Dentz, M., Icardi, M., Hidalgo, J.J., 2018. Mechanisms of dispersion in a porous medium. J. Fluid Mech. 841, 851–882.
Emami Meybodi, H., Hassanzadeh, H., 2011. Hydrodynamic dispersion in steady buoyancy-driven geological flows. Water Resour. Res. 47 (12).
Feng, G., Xu, T., Gherardi, F., Jiang, Z., Bellani, S., 2017. Geothermal assessment of the Pisa plain, Italy: coupled thermal and hydraulic modeling. Renew. Energy 111, 416–427.
John, A.K., Lake, L.W., Bryant, S.L., Jennings, J.W., 2010. Investigation of mixing in field-scale miscible displacements using particle-tracking simulations of tracer floods with flow reversal. Soc. Pet. Eng. J. 15 (03), 598–609.
Khait, M., Voskov, D., 2018. Operator-based linearization for efficient modeling of geothermal processes. Geothermics 74, 7–18.
Lake, L.W., Hirasaki, G.J., 1981. Taylor's dispersion in stratified porous media. Soc. Pet. Eng. J. 21 (04), 459–468.
Lake, L., Johns, R.T., Rossen, W.R., Pope, G.A., 2014. Fundamentals of Enhanced Oil Recovery. Society of Petroleum Engineers, Richardson, Texas.
Murphy, H.D., Tester, J.W., Grigsby, C.O., Potter, R.M., 1981. Energy extraction from fractured geothermal reservoirs in low-permeability crystalline rock. J. Geophys. Res.: Solid Earth 86 (B8), 7145–7158.
Major, M., Daniilidis, A., Hansen, T.M., Khait, M., Voskov, D., 2023. Influence of process-based, stochastic and deterministic methods for representing heterogeneity in fluvial geothermal systems. Geothermics 109, 102651.
Nakayama, A., Kuwahara, F., Kodama, Y., 2006. An equation for thermal dispersion flux transport and its mathematical modelling for heat and fluid flow in a porous medium. J. Fluid Mech. 563 (1), 81–96.
Norouzi, A.M., Gluyas, J., Babaei, M., 2022. CO2-plume geothermal in fluvial formations: a 2D numerical performance study using subsurface metrics and upscaling. Geothermics 99, 102287.
Oldenburg, C.M., Pruess, K., 1998. Layered thermohaline convection in hypersaline geothermal systems. Transp. Porous Media 33 (1), 29–63.
Ortan, A., Quenneville-Bélair, V., Tilley, B.S., Townsend, J., 2009. On Taylor dispersion effects for transient solutions in geothermal heating systems. Int. J. Heat Mass Transfer 52 (21-22), 5072–5080.
Park, B.H., Lee, B.H., Lee, K.K., 2018. Experimental investigation of the thermal dispersion coefficient under forced groundwater flow for designing an optimal groundwater heat pump (GWHP) system. J. Hydrol. 562, 385–396.
Pearce, P., Daou, J., 2014. Taylor dispersion and thermal expansion effects on flame propagation in a narrow channel. J. Fluid Mech. 754, 161.
Plumb, O.A., Whitaker, S., 1988. Dispersion in heterogeneous porous media: 1. Local volume averaging and large-scale averaging. Water Resour. Res. 24 (7), 913–926.
Robert, S., Pasquier, P., Nguyen, A., 2022. Impact of layered heterogeneity on thermal response test interpretation performed on a standing column well operated without bleed. Geothermics 101, 102353.
Rühaak, W., Guadagnini, A., Geiger, S., Bär, K., Gu, Y., Aretz, A., Homuth, S., Sass, I., 2015. Upscaling thermal conductivities of sedimentary formations for geothermal exploration. Geothermics 58, 49–61.
Sbai, M.A., Larabi, A., 2023. Analyzing the relationship between doublet lifetime and thermal breakthrough at the Dogger geothermal exploitation site in the Paris basin using a coupled mixed-hybrid finite element model. Geothermics 114, 102795.
Seibert, S., Prommer, H., Siade, A., Harris, B., Trefry, M., Martin, M., 2014. Heat and mass transport during a groundwater replenishment trial in a highly heterogeneous aquifer. Water Resour. Res. 50 (12), 9463–9483.
Tang, D.W.S., van der Zee, S.E.A.T.M., 2021. Dispersion and recovery of solutes and heat under cyclic radial advection. J. Hydrol. 602, 126713.
Taylor, G.I., 1953. Dispersion of soluble matter in solvent flowing slowly through a tube. Proceedings of the Royal Society of London. Series A. Mathematical and Physical Sciences 219 (1137), 186–203.
Thomas, H., Brigaud, B., Blaise, T., Zordan, E., Zeyen, H., Catinat, M., Fleury, M., 2023. Upscaling of geological properties in a world-class carbonate geothermal system in France: from core scale to 3D regional reservoir dimensions. Geothermics 112, 102719.
van Nieuwkerk, P., 2022. MSc thesis. Delft University of Technology.
Wang, Q., Shi, W., Zhan, H., Xiao, X., 2020b. New model of single-well push-pull thermal test in a fracture-matrix system. J. Hydrol. 585, 124807.
Wang, Y., Voskov, D., Khait, M., Bruhn, D., 2020a. An efficient numerical simulator for geothermal simulation: a benchmark study. Appl. Energy 264, 114693.
Wang, Y., Voskov, D., Khait, M., Saeid, S., Bruhn, D., 2021. Influential factors on the development of a low-enthalpy geothermal reservoir: a sensitivity study of a realistic field. Renewable Energy 179, 641–651.
Wikipedia, 2016. Taylor dispersion. Available at. https://de.wikipedia.org/wiki/Taylor-Dispersion.
Willems, C.J., Nick, H.M., Weltje, G.J., Bruhn, D.F., 2017. An evaluation of interferences in heat production from low enthalpy geothermal doublets systems. Energy 135, 500–512.
Yan, H., Xie, H., Nikolaev, P., Ding, H., Shi, Y., Chen, Y., 2022. Analytical model for steady-state solute diffusion in non-isothermal fractured porous media. J. Hydrol., 128872